Towards a surface consistent match filter (SCMF) for time-lapse processing

Mahdi Almutlaq and Gary F. Margrave

ABSTRACT

This paper presents a new idea for designing a match filter for processing time-lapse seismic data in a surface consistent manner. We extend the surface consistent data model to the case of designing matching filters to equalize two seismic surveys in the least-square sense. The frequency-domain surface-consistent design equations are similar to those for surface consistent deconvolution except that the data term is the spectral ratio of two surveys. To test this concept we have built a time-lapse synthetic dataset (baseline and monitor) whose subsurface (the reservoir) is unchanging but which show surface-consistent variability. Our synthetic dataset models acquisition over a simple stratigraphic reservoir in both summer and winter. Initial results are encouraging but suggest that our software is not yet optimal.

INTRODUCTION

The term "surface-consistent" is widely used in exploration geophysics as desirable feature of a seismic data algorithm. Some of the algorithms formulated as being surface-consistent are deconvolution, amplitude corrections, velocity analysis, and static corrections. The wavelet recorded on a seismic trace can be looked at as the convolution of four-components: the trace's source signature, receiver impulse response, an offset response, and a midpoint response (Taner and Koehler, 1981). This four-component decomposition is known as the surface-consistent model, even though only two of the four components (source and receiver) are consistent with the actual surface locations (Cary and Lorentz, 1993). This model has been suggested by Taner and Koehler, 1981, and implemented by several authors to attain more accurate and stable deconvolution filters, amplitude and phase adjustments from the seismic data, statics estimation, noise reduction and velocity analysis (Morely and Claerbout, 1983; Levin, 1989; Cambois and Stoffa, 1992; Cary and Lorentz, 1993).

The four-component decomposition can be implemented in both time (Levin, 1989) where it is supposed to be more robust or in frequency (log/Fourier) domain where the problem becomes linear (Taner and Coburn, 1980; Morely and Claerbout, 1983; Cambois and Stoffa, 1992). Many of the advantages of working in the frequency domain over the time domain are discussed by Cambois and Stoffa (1992).

This paper examines the use of the four-component surface-consistent method to accurately process a repeated seismic survey for reservoir monitoring. There are many ways of matching and then taking the difference between two repeated seismic surveys. Details of matching methods have been discussed by Jack (1998) in his SEG short course. Time-lapse seismic surveys measure some primary reservoir properties, such as reservoir pore pressure, reservoir pore fluids, reservoir temperature, and some secondary reservoir properties such as reservoir fractures, reservoir compaction, density and porosity (Jack, 1998). Seismic data can observe some of the changes that occur with time

such as times on surface seismic data, amplitudes, velocities, frequencies and phase (Jack, 1998). Some of the undesirable changes that happen with time are ambient noise, acquisition parameters (source arrays, receiver arrays, positioning system, ...etc) and processing parameters (Jack, 1998).

Many of the above mentioned issues that face time-lapse seismic technology have not been resolved completely. For example, would positioning receivers permanently solve the repeatability problem and if so how about the source positioning? To what extent should the new survey mimic the original one? Are there any problems in processing such data that might overcome some of these challenges? All of these questions are reasonable and have been asked many times before. In this research, we introduce an innovative approach to solve some of the issues of time-lapse surveys. This method can simply be described as a surface consistent match filter. First, we will describe the theoretical background of this method and then introduce the new math and how it can be applied. Second, we will describe the synthetic model used to generate seismic data for the experiment. Finally, preliminary results will be discussed and some insights on the way forward will be presented.

THEORY

The four-component surface consistent decomposition

Taner and Kohler (1980) and Morley and Claerbout (1983) modeled the seismic trace $p(t)$ as the convolution of four operators:

$$p_{ijkl}(x_i, x_j, x_k, x_l, t) = s_i(x_i, t) * r_j(x_j, t) * h_k(x_k, t) * y_l(x_l, t) * a(t) \qquad (1)$$

where we assume a 2D seismic line and the left hand side of equation 1, $p_{ijkl}(x_i, x_j, x_k, x_l, t)$, represents the seismic trace as a function of the source (s), receiver (r), offset (h), subsurface midpoint (y), average spectrum for the entire line (a), space (x) and time (t). * is convolution in time. On the other side of equation (1): $s_i(x_i, t)$ represents the source consistent effects, $r_j(x_j, t)$ represents receiver consistent effects, $h_k(x_k, t)$, $k = |i - j|$ represents offset consistent effects, and $y_l(x_l, t)$, $l = (i + j)/2$ represents midpoint consistent effects (as well as information on reflectivity). Note that the average spectrum in Equation 1 is a function of time only (this term is not used in the coding of this study or in the subsequent equations but we plan to add it in the next stage of the work).

Equation 1 can be formulated in the frequency domain such that

$$P_{ijkl}(\omega) = S_i(\omega)R_j(\omega)H_k(\omega)Y_l(\omega), \qquad (2)$$

where we use capital letters to denote the Fourier transforms of the time-domain functions in equation 1. For simplicity of writing these equations, we have dropped the space term (x). Cary and Lorentz (1993) took the logarithms of both sides of equation 2 and considered the real parts only, which contains the log-amplitude information

$$\ln\left(P_{ij}(\omega)\right) = \ln\left(S_i(\omega)\right) + \ln\left(R_j(\omega)\right) + \ln\left(H_k(\omega)\right) + \ln\left(Y_l(\omega)\right). \quad (3)$$

Constructing the surface consistent match filter

In this paper, we are considering the applications of equation 2 above for two repeated seismic surveys such that

$$P_{ij1}(\omega) = S_{i1}(\omega)R_{j1}(\omega)H_{k1}(\omega)Y_{l1}(\omega) \quad (4a)$$

$$P_{ij2}(\omega) = S_{i2}(\omega)R_{j2}(\omega)H_{k2}(\omega)Y_{l2}(\omega). \quad (4b)$$

Taking the ratio of both surveys in equation 4 we get:

$$P_{ij2}(\omega)/P_{ij1}(\omega) = S_{i2}(\omega)R_{j2}(\omega)H_{k2}(\omega)Y_{l2}(\omega)/S_{i1}(\omega)G_{j1}(\omega)H_{k1}(\omega)Y_{l1}(\omega). \quad (5)$$

For simplicity, we can rename $S_i = S_{i2}/S_{i1}$ and similarly for all the other terms. The general form of equation 5 can be written as

$$P_{ij2}(\omega)/P_{ij1}(\omega) = S_i(\omega)R_j(\omega)H_k(\omega)Y_l(\omega). \quad (6)$$

Similarly, if we take the logarithms of both sides of equation 6 we obtain an analogous form of equation (3) above but here we have included a ratio term for the data spectra

$$\ln\left(P_{ij2}(\omega)/P_{ij1}(\omega)\right) = \ln\left(S_i(\omega)\right) + \ln\left(R_j(\omega)\right) + \ln\left(H_k(\omega)\right) + \ln\left(Y_l(\omega)\right). \quad (7)$$

Each of the components (source, receiver ... etc) in equation 6 is an operator or filter that contains the variations due to near surface geology. These operators are applied (multiplication in frequency domain or convolution in time domain) to the survey in the denominator of the ratio ($P_{ij1}(\omega)$) in order to match it to the survey in the numerator. Equation 7 linearly relates the parameters *S*, *R*, *H*, and *Y* to the data P_2/P_1. If NS is number of sources, NR is number of receivers, NC is number of channels, NH is number of offsets, and NY is number of CDP's then equation (7) is going to have NS x NC linear equations and NS + NR + NH + HY unknowns (Cary and Lorentz, 1993).

Following Wiggins et al. (1976), equation (6) can be written:

$$P_{ij2}(\omega)/P_{ij1}(\omega) \rightarrow \boldsymbol{p}(\omega) = \boldsymbol{G}\boldsymbol{x}(\omega) \; with \; \boldsymbol{x}(\omega) = \begin{pmatrix} \boldsymbol{s}(\omega) \\ \boldsymbol{r}(\omega) \\ \boldsymbol{h}(\omega) \\ \boldsymbol{y}(\omega) \end{pmatrix}, \quad (8)$$

where $\boldsymbol{p}$ is the data vector (in this case the log of the ratio of the amplitude spectrum of the traces in both surveys), $\boldsymbol{x}$ represents the unknown parameter vectors (S_i, R_j, H_k, and Y_l in frequency domain) and $\boldsymbol{G}$ is the geometry matrix which contains the positions of the four-components described in equation (6). The geometry matrix in this study is illustrated in Figure 1 where the positions S, R, H, and Y are represented by 1's. NS in this study is 26, NR is 251, NH is 101, and NY is 501. Therefore we have in total 879 columns of unknowns. The number of linear equations (number of rows) are NS x NC which is 26 x 101. The explicit structure of the system described in equation 8 can be seen in Figure 2. We cannot obtain a unique solution to this system of linear equations

(also said to be an overdetermined system) since the geometry matrix ***G*** has more rows (data) than columns (unknowns). Taking the SVD of ***G*** shows clearly some zero singular values as illustrated in Figure 3. This matrix is specific to the geometry used for this study which will be described in details in the synthetic model section below.

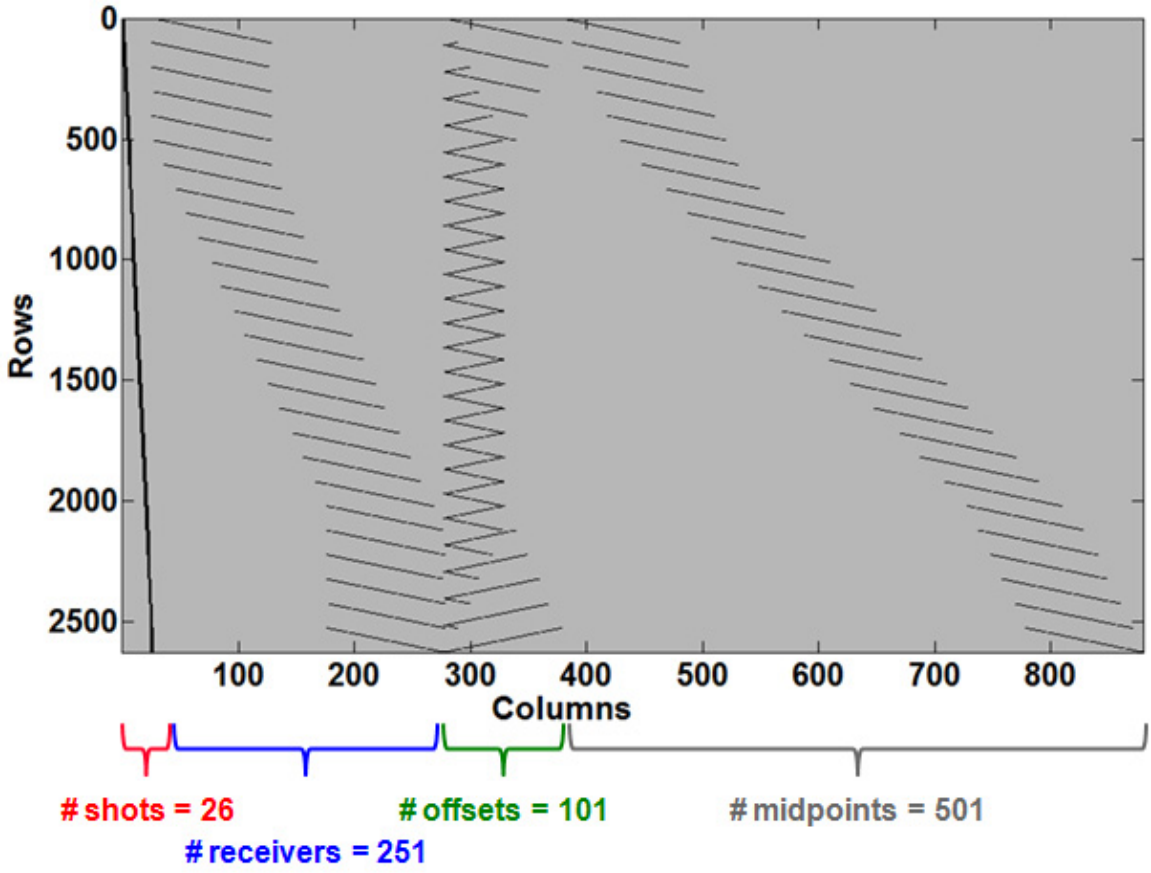

FIG. 1: The geometry matrix ***G*** described in equation (8). The first 26 columns are for the shot positions, then there are 251 columns representing the receiver positions, then there are 101 columns for the offset positions, and finally there are 501 columns for the midpoint positions.

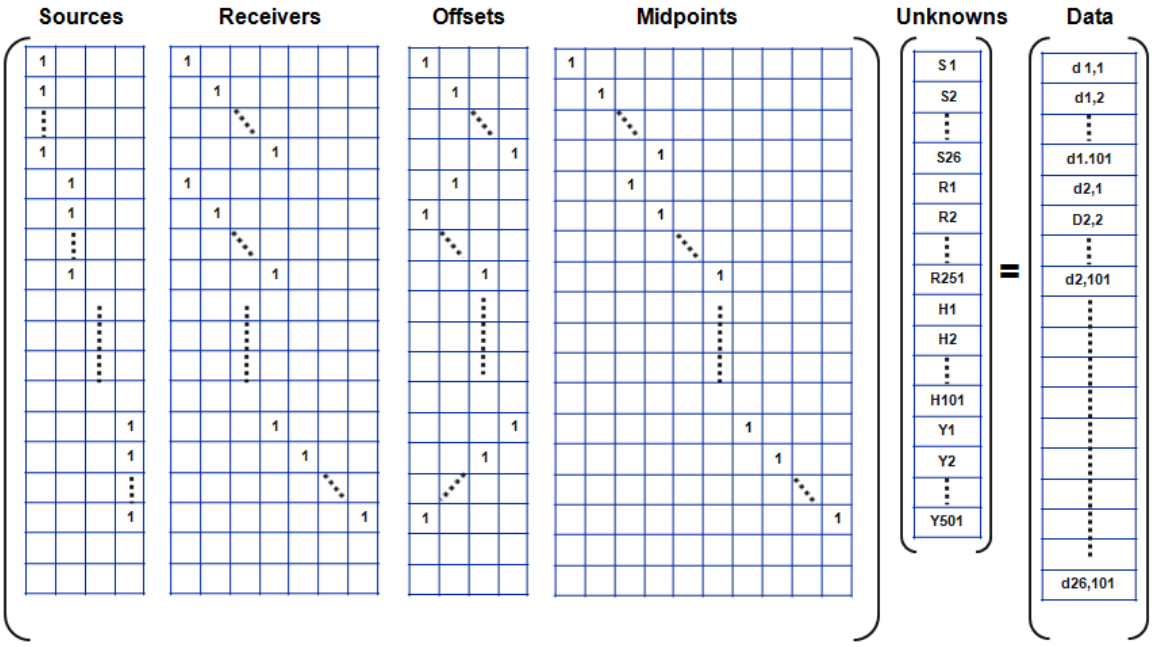

FIG. 2: The structure of the system of linear equation described in equation 8.

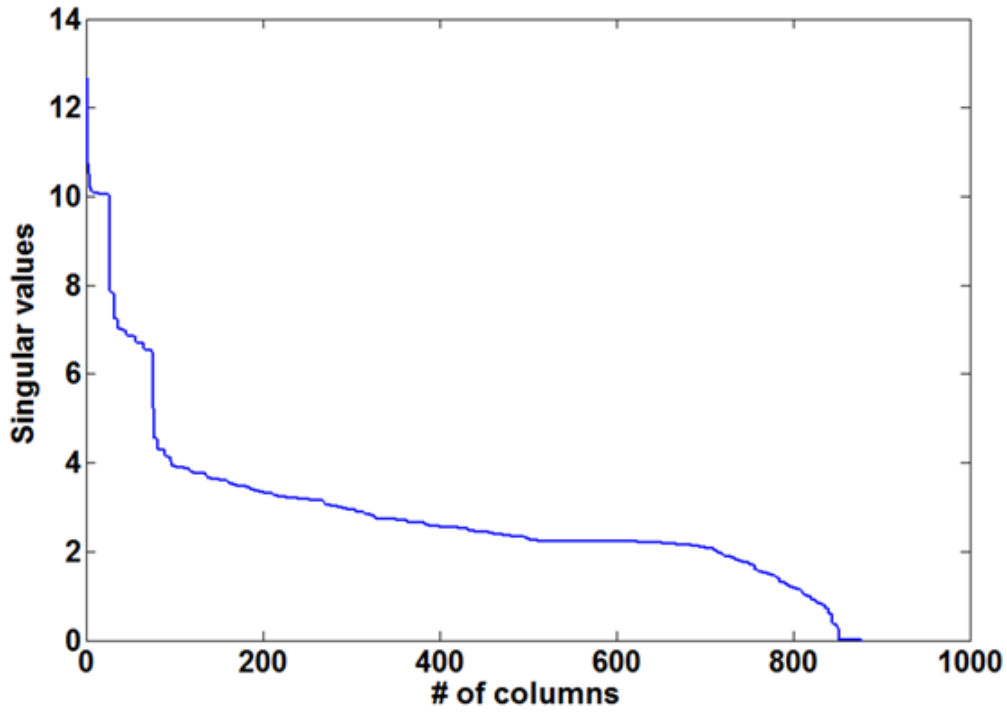

FIG. 3: Singular values of the geometry matrix ***G***. Note that the last values of this diagonal matrix are zeros.

METHODOLOGY AND DISCUSSION

Constructing the synthetic model

The earth model constructed for this experiment is a simple 2.5km wide and 1km thick (Figure 4) 2D model of a stratigraphic reservoir. The model consists of four layers and a reservoir unit, 500m wide and 20m thick, between layers three and four. The velocity is homogeneous in each layer except for the first one. The velocity of the first layer is variable with lateral distance (x-axis) but constant with depth (z-axis). The base of the first layer is undulating to resemble a real earth near surface model with an average thickness of about 50m (Figure 5). We have generated two earth models, a summer season velocity model (for baseline survey) and a winter season velocity model (for monitor survey). The difference between both models is in the near surface layer where the velocity increases for the winter season model by about 20% compared to the summer season velocity model. Also in the near surface layer, we model a simple attenuation process which is more severe in the summer than in the winter.

Our next step is modeling the seismic data. Figure 6 illustrates the acquisition geometry of the 2D seismic line. The maximum length of the line is 2.5km. There are 26 shots with spacing of a 100m and 100 receivers per shot with a spacing of 10m. The maximum record length is 1s with a 4ms sampling interval.

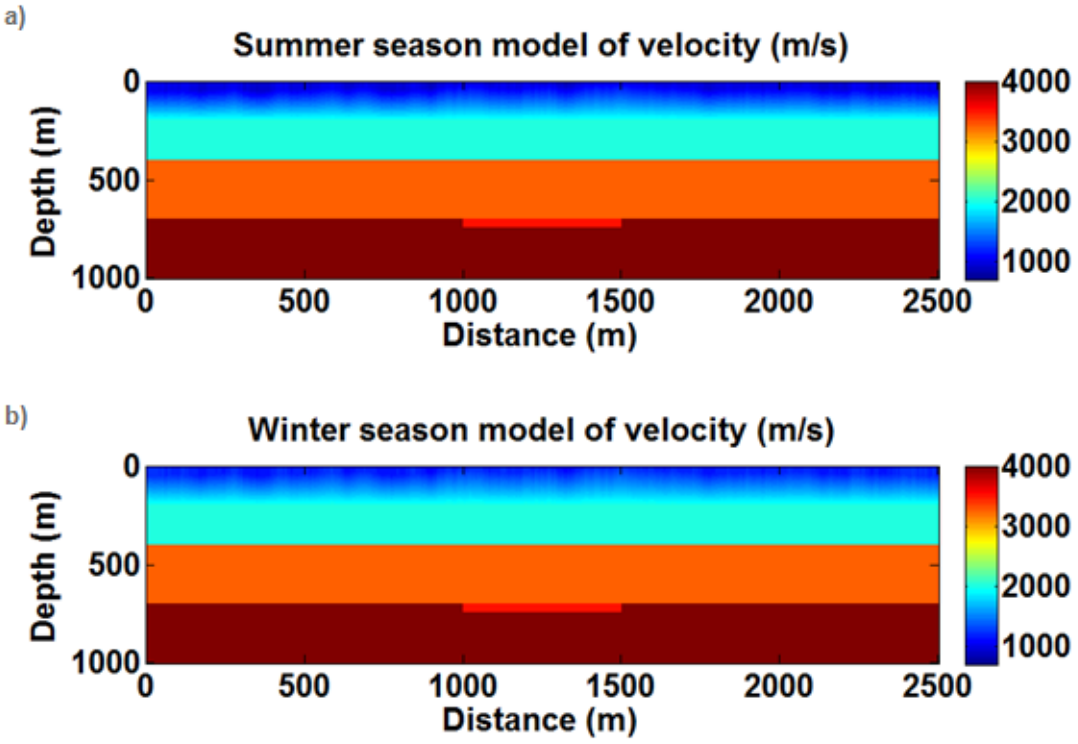

Fig. 4: A simple four layer model with a reservoir unit between layers 3 and 4. Both models are similar except at the first layer where in the summer season (baseline survey) (a) the velocity is lower by about 30% compared to the winter season (monitor survey) velocity model (b).

Given the above sources and receivers configuration, an acoustic finite difference algorithm is used to generate two sets of shot records, summer season shot records and winter season shot records. We used a minimum phase wavelet with a dominant source frequency of 20 Hz. In addition to the variations of velocity in the geologic model, source strength and receiver coupling are made variable for both seasonal surveys (Figure 7a and b). Also we have included an attenuation variation for both seasons, where the attenuation is constant with depth but variable in the x-axis direction and the winter attenuation is less than that of the summer season (Figure 7c). We model this attenuation as a simple source/receiver consistent wavelet effect. Figure 8 illustrates a comparison of the same shot record (exact shot location and exact geophones) for both summer and winter surveys. To better visualize the variations in the data, we extract the average amplitude by taking a time window around one of the middle reflectors and plotting this on a source/receiver chart (Figure 9). The extracted amplitudes show a source/receiver pattern as vertical and horizontal stripes on the plot. These consistent signatures of sources and receivers are the ones we are hoping to reduce using the operators or filters designed in this next section.

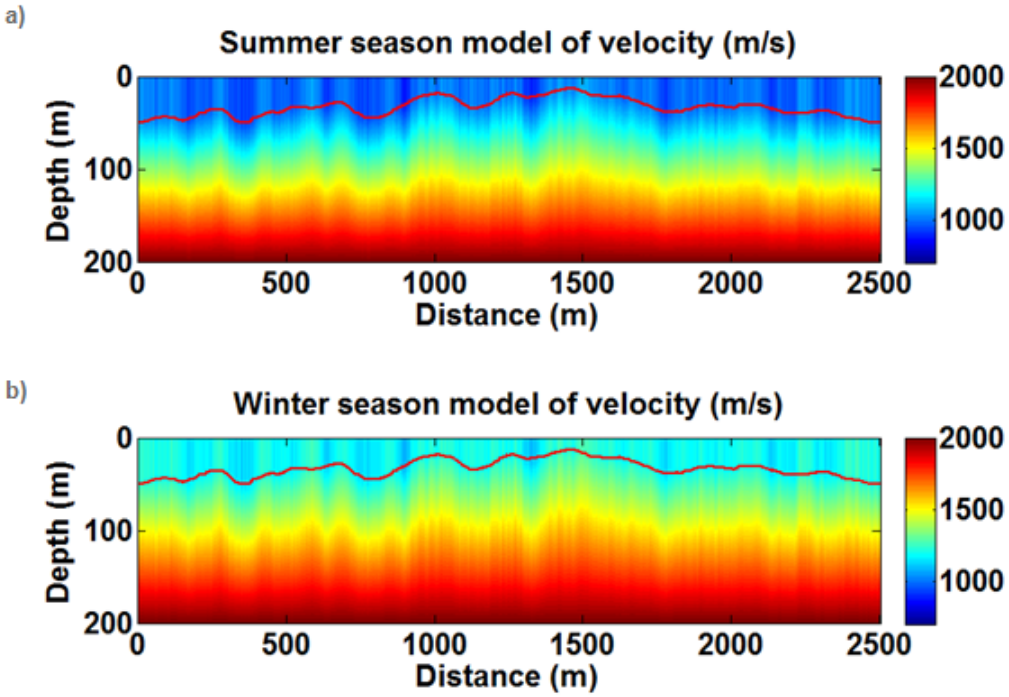

FIG. 5: A zoom in to the first 200m of Figure 4 to illustrates more details of the near surface layer. The red line displays the bottom of the near surface layer. Note the increase in velocity from the summer model (a) to the winter model (b). Note also that the boundary between this near surface layer and the next one is smooth because the velocity is linearly increasing to the next boundary.

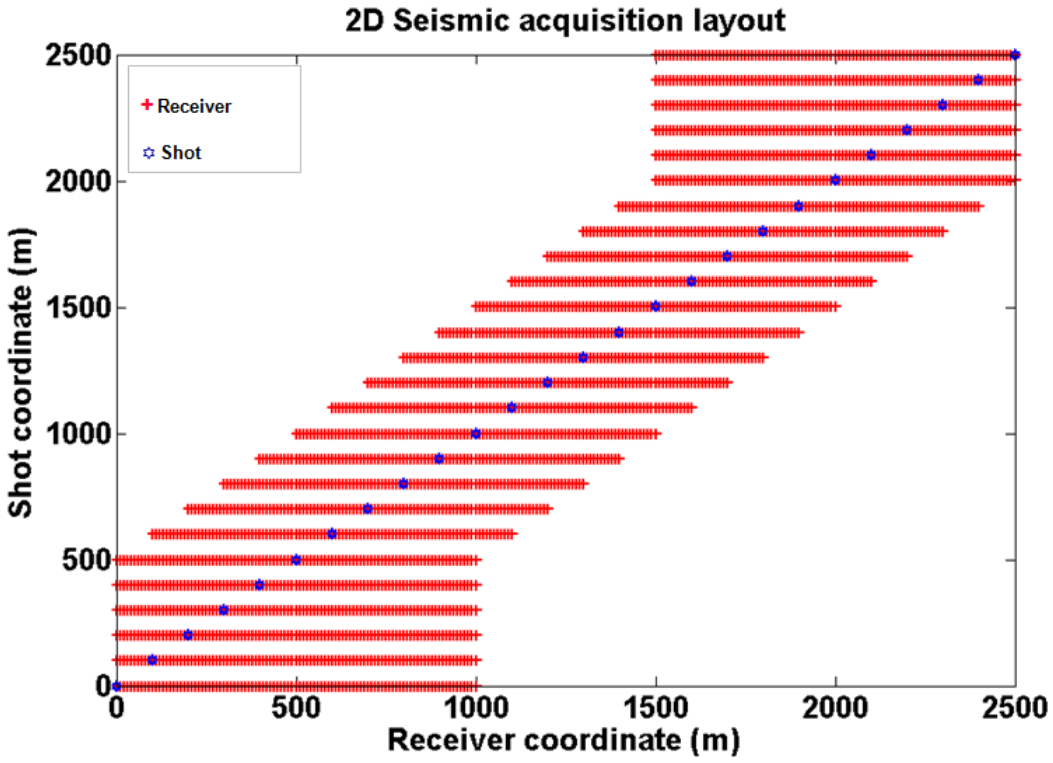

FIG. 6: Illustrates the geometry array of the 2D seismic acquisition.

Interpretation of the four surface-consistent operators

The source and receiver operators

The hypothesis of the surface consistent decomposition assumes that the source-consistent terms contains all the effects of the source signature and the near surface conditions around each shot on the recorded data (Cary and Lorentz, 1993). Similarly, the receiver-consistent terms collects all the effects of the receiver instrument response and the near surface conditions surrounding each receiver on the recorded data (Cary and Lorentz, 1993). Our goal is to process the data such that these effects are equalized between the data.

Figure 10a illustrates a comparison between the ratio of the source strength in summer season to the source strength in winter season and comparing that to the RMS of the source operator after taking the logarithm of the ratio of the amplitude spectrum of both surveys. In a similar fashion, Figure 10b shows the receiver variations comparison. Notice that the shot operators correlates well with the known variations in the sources. Likewise, the receiver components compares well with the known variations in the receivers.

The shot and the receiver components, extracted from the log-amplitude spectra then inverse Fourier back to time, are shown in Figure 11a and b, consecutively. Considering that this is still a work in progress, the results are encouraging. As mentioned previously, both the shot and receiver operators correlate well with the known variations in shots and receivers. The receiver operator shows more noise when compared to the shot operator.

At this step, all the filters have mixed phases, where baseline and monitor surveys are minimum phase and the operators are zero phase. After applying inverse Fourier transform to the operators (transform operators to time domain), the data are wrapped. To rid the data of this characteristic, we shifted the rows of each column of the operator matrix such that the maximum spectrum is in the middle. This introduces undesired results since the operator becomes a non-causal one. A detail discussion on the consequences of converting filters back to minimum phase will be discussed in the results section.

The offset operator

It is difficult at this stage to judge the effectiveness of the offset operator shown in Figure 11c. Because of the additive noise caused by the non-causal operator, in addition to the coherent noise present in the data, higher amplitudes can be seen scattered around the central maximum amplitude spectrum. It can also be noted from this operator that amplitudes are present in the near offsets compared to low amplitudes in the far offset.

The midpoint operator

Figure 11d shows the midpoint operators. We notice from this plot that we have some pattern that illustrates symmetry around the central part of the operator. At this moment, it is difficult to explain the behaviour of this operator. In general, this operator is known to collect much more noise than in the other components and to overcome this noise problem a smoothing is performed (Cary and Lorentz, 1993). No smoothing is applied to this operator or any of the other operators in this study.

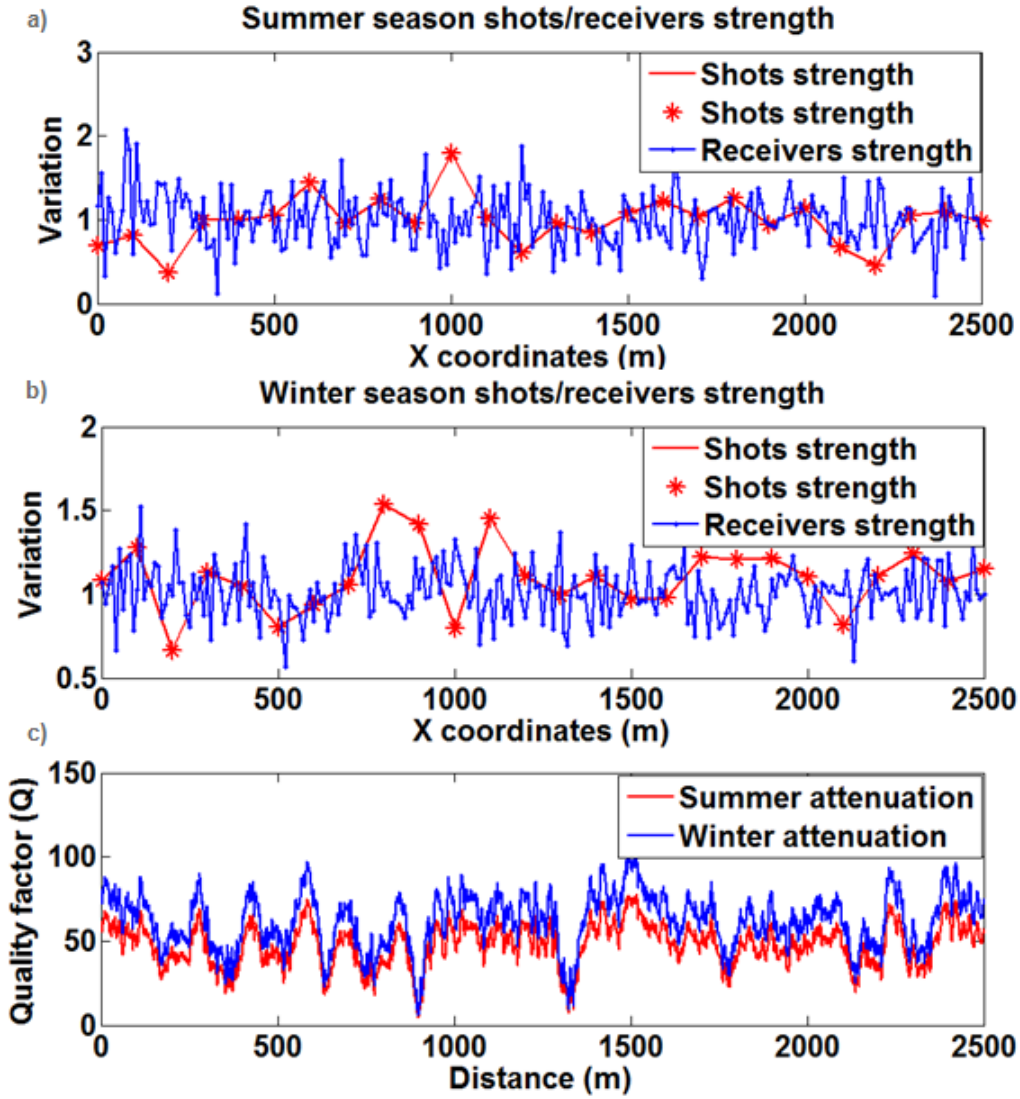

FIG. 7: Source and receiver strengths variations for both summer season acquisition (a) and the winter season acquisition (b). Attenuation variation is shown in (c) for both the summer and winter seasons.

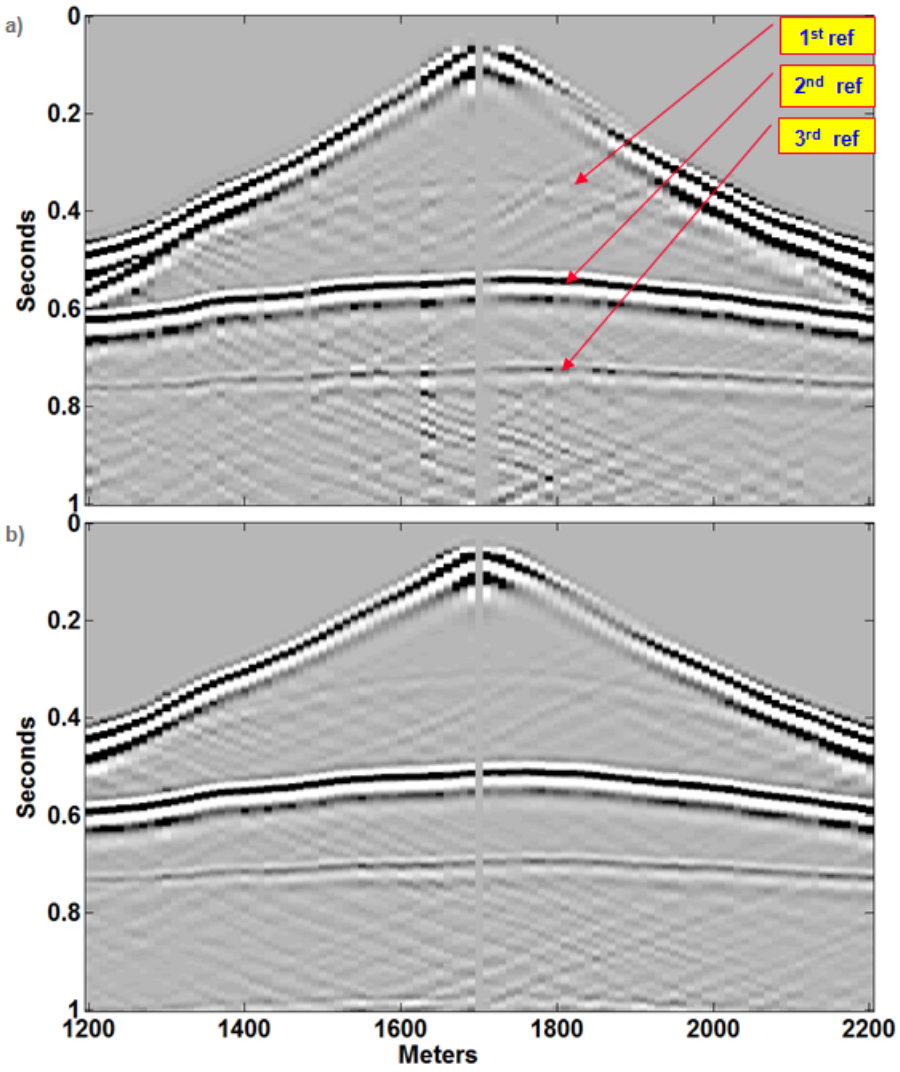

FIG. 8: Illustrates a comparison of the same shot record (exact shot location and exact geophones) for both summer (a) and winter (b) surveys (shot # 17). The three reflectors are denoted in (a).

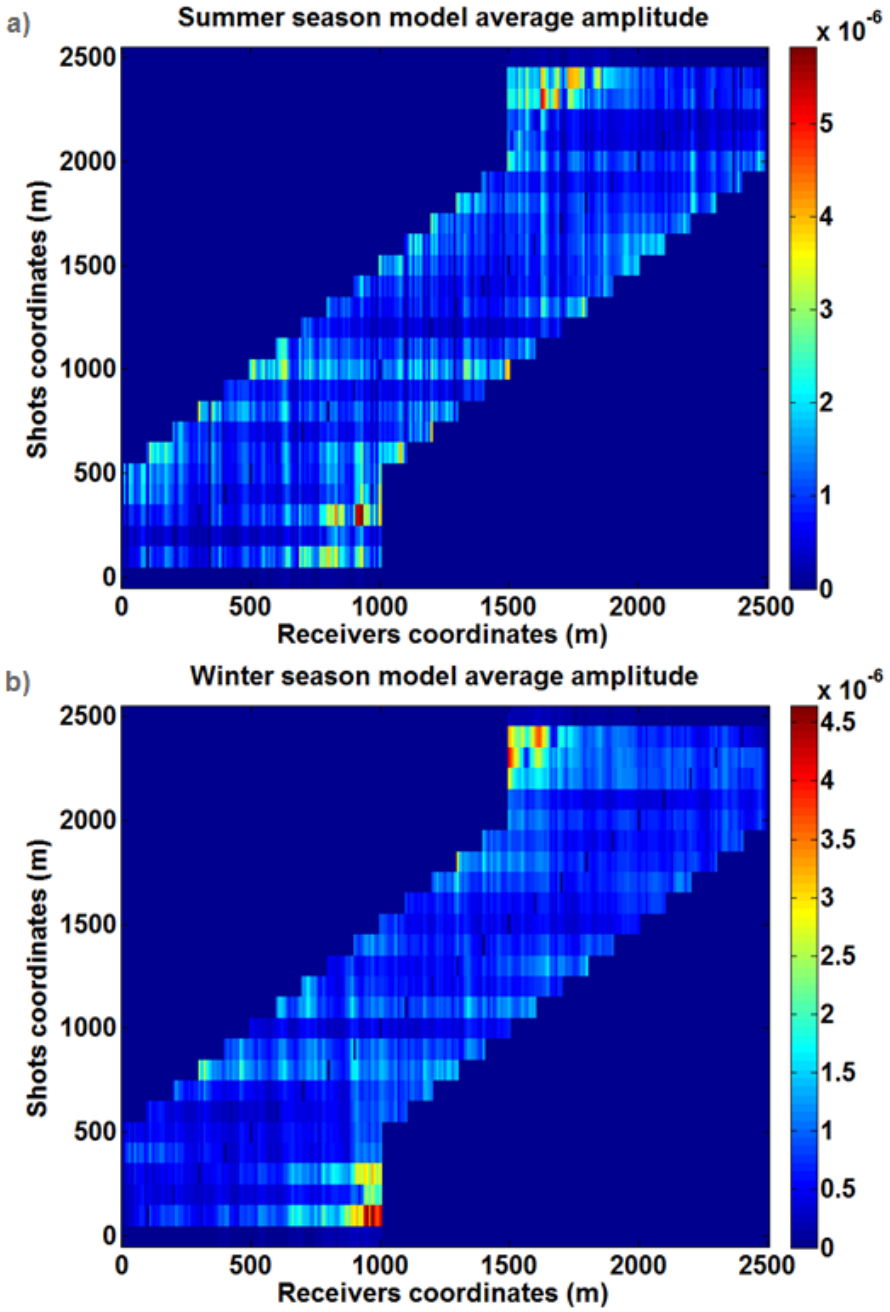

FIG. 9: Shows the extracted average amplitude which is taking from a time window around second reflector. The extracted amplitude shows a consistent pattern for some of the receivers and the sources for both the summer season survey (a) and the winter season survey (b).

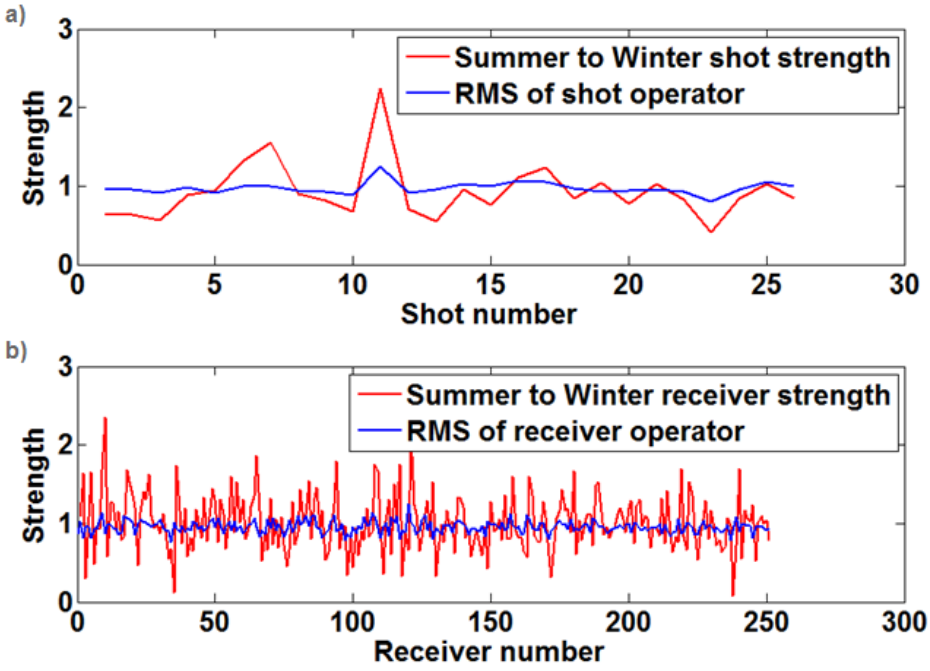

FIG. 10: Illustrates a comparison between the ratio of the source strength in summer season to the source strength in winter season and comparing that to the RMS of the source operator after taking the logarithm of the ratio of the amplitude spectrum of both surveys (a). Similarly, (b) shows the receiver variations comparison. Note the good correlation.

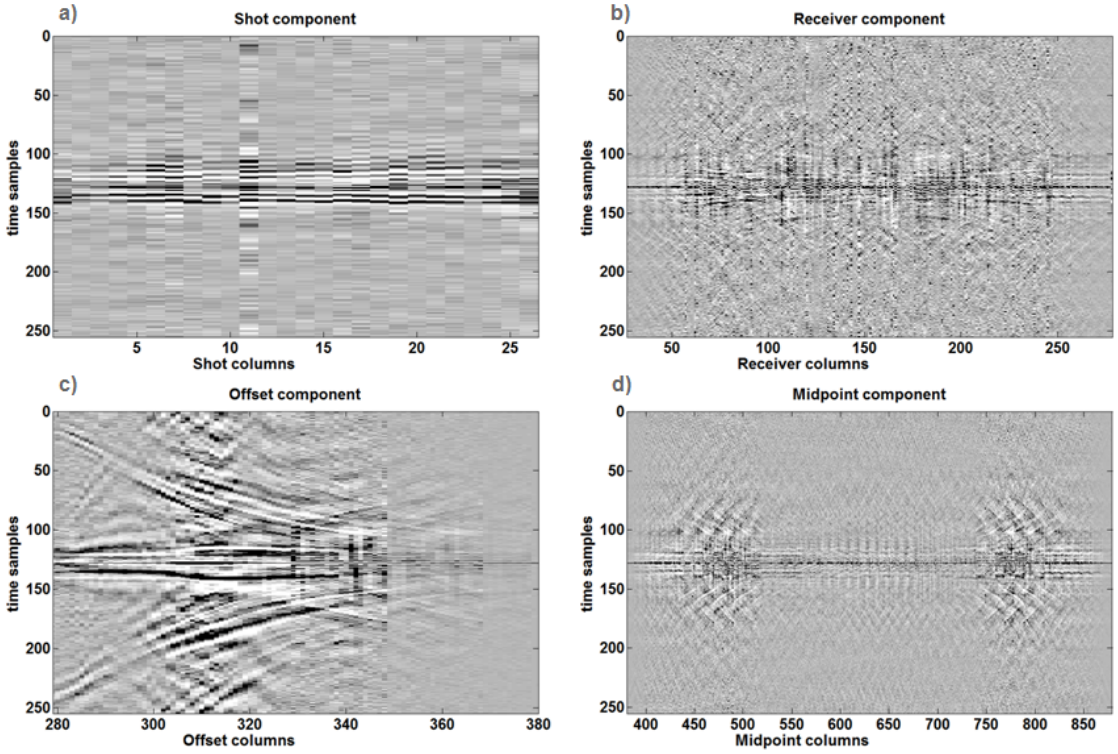

FIG. 11: Shows the shot component (a), receiver component (b), offset component (c), and midpoint component (d).

RESULTS

We have applied the individual operators (source, receiver, offset, and midpoint) to the winter survey shot records. Figure 12a shows shot record # 17 from the winter survey with the shot operator applied. Note the undesirable artefacts produced by the non-causal operator above the first break. The deep data are masked by linear noise that is more likely produced by this effect as well. Similarly, Figure 12b demonstrates the application of the receiver filter to the same shot record. The result is not very encouraging giving the noise level. Figure 12c is both source and receiver filters applied to the same shot record where the noise level is amplified. A more diagnostic look at the data is illustrated in Figure 12d which consists of a single trace from shot record # 17 comparing the summer survey, the winter survey, and the source and receiver operators applied to the winter survey.

Figure 12d illustrates clearly that having a mixed phase match filter is not optimum. Theoretically, the zero phase operator has an important advantage over minimum phase where it can easily estimate the time delays. Unfortunately, this advantage could not be obtained in Figure 12. Figure 13 illustrates the same shot but converted to minimum phase operator. The result has less noise as expected and a similar estimate of the amplitude however time delay cannot be estimated. Figure 14 shows that when solving a match filter for two traces we estimate the time delay (in addition to the amplitude). This time delay is lost if we convert the operator into a minimum phase one.

At the moment, we have two challenges: 1) annoying artefacts due to non-causal operator and 2) unresolved time delay. We are assuming, although very difficult to conclude yet, that the amplitudes of the monitoring survey are matched to the baseline survey. To overcome these problems, we plan to solve the match filters as a mixed phase. We then estimate the time delay separately. We plan to convert the operators back to minimum phase and then cross correlate the traces of the baseline survey to the traces with mixed phase match filter. The time delay estimated from this cross correlation will be removed from the matched data.

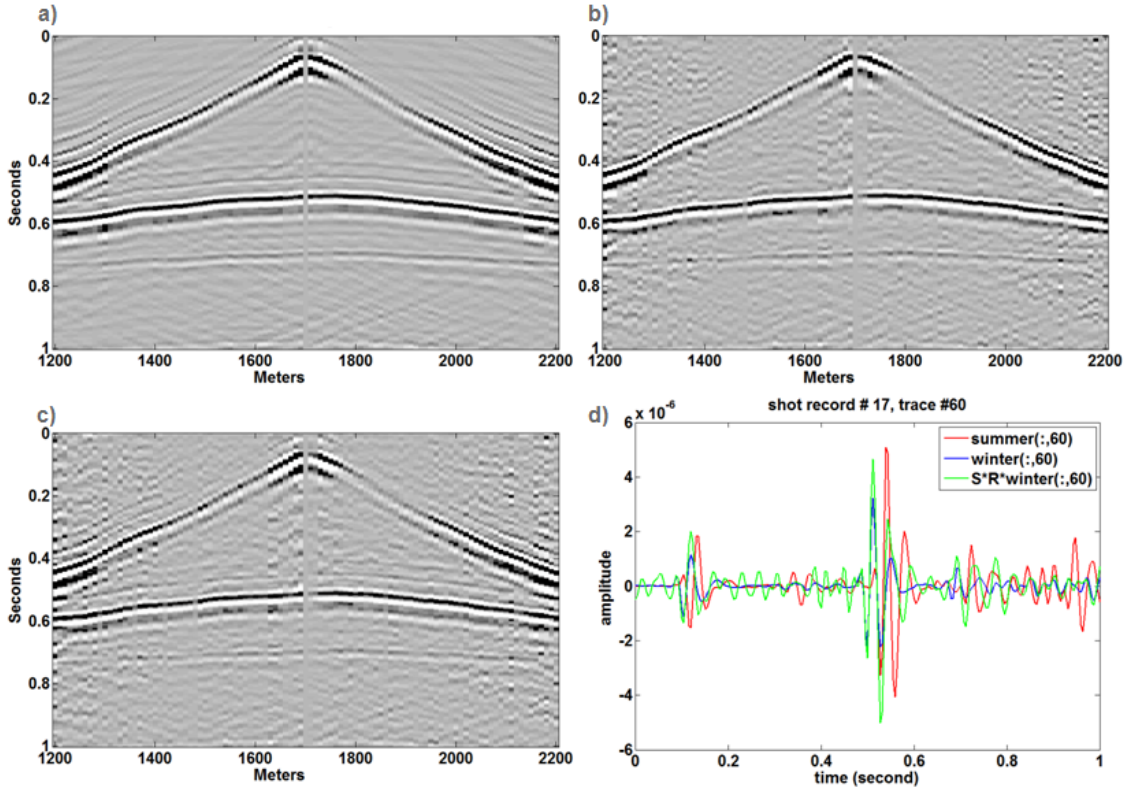

FIG. 12: (a) Shows shot record # 17 from the winter survey with the shot operator applied. (b) Illustrates the application of the receiver filter to the same shot record. (c) Both source and receiver filters are applied to the same shot record and note that the noise introduced by the non-causal operator above first-break. (d) Consists of a single trace from shot record # 17 comparing the summer survey (red), the winter survey (blue), and the source and receiver operator applied to the winter survey (light green). The result of applying both filters is not yet perfect because of the unresolved time delay and the increase level of noise.

CONCLUSIONS AND FUTURE WORK

In conclusion, we have demonstrated that theoretically a surface consistent match filter that is useful for processing time lapse seismic data is possible. This hypothesis is analogous to the well known four-component surface consistent deconvolution except that it considers two repeated seismic surveys instead of just one. Since this is a work in progress, we have managed to build a work flow that generates the four surface consistent components. We have built a very useful synthetic dataset that contains a baseline and a monitor survey with surface consistent, seasonal variations built into the model. This will allow us to benchmark our code. We have demonstrated, using our synthetic data, that obtaining the four operators is possible. These operators are still not fully useful due to problems in estimating the time delay and noise level caused by the non-causal operator.

Therefore, the future work will include fixing the problems discussed in the result section above. Once we have a working four-components surface consistent match filter for the available synthetic data, application to a real dataset will be the ultimate test.

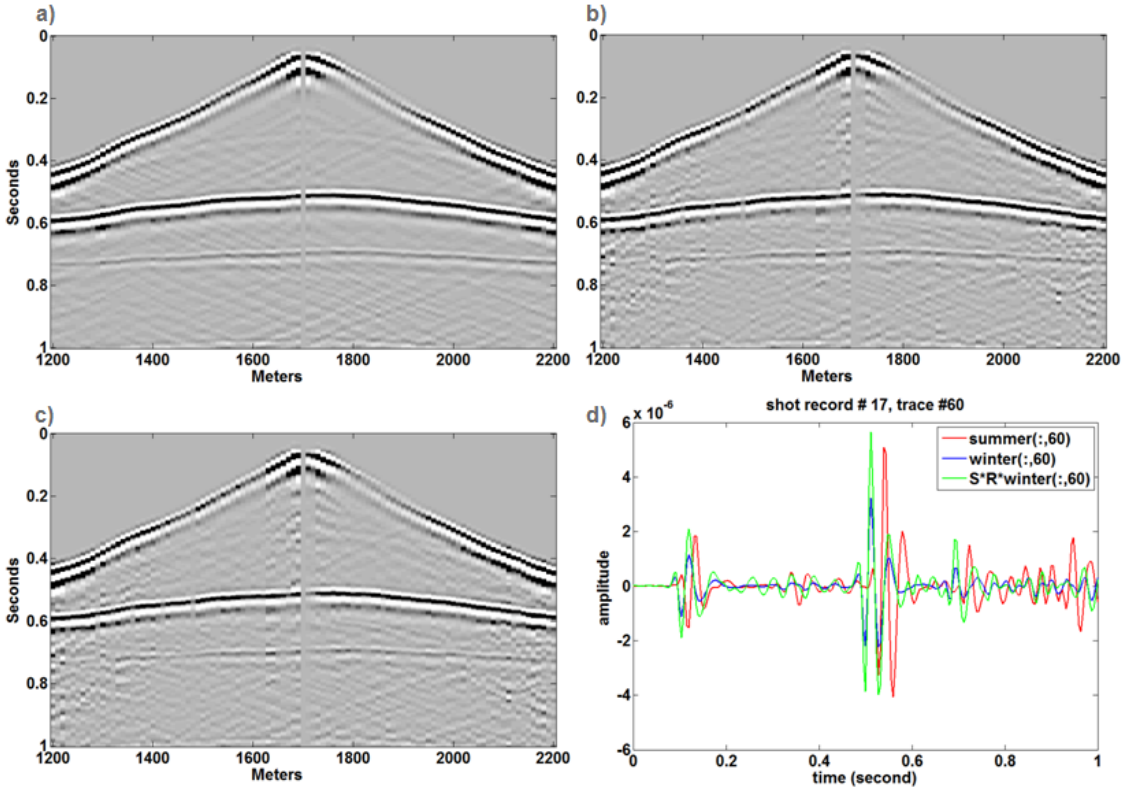

FIG. 13: These are the same filters shown in Figure 12 but converted to minimum phase operators. a) Shows shot record # 17 from the winter survey with the shot operator applied. (b) Illustrates the application of the receiver filter to the same shot record. (c) Both source and receiver filters are applied to the same shot. (d) Consists of a single trace from shot record # 17 comparing the summer survey (red), the winter survey (blue), and the source and receiver operator applied to the winter survey (light green).

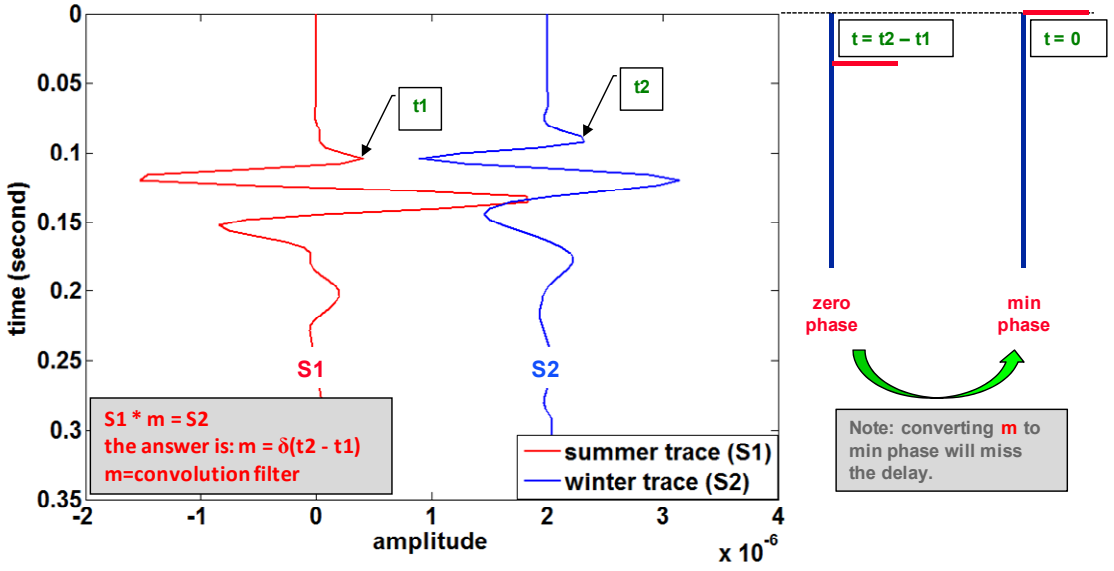

FIG. 14: Demonstrates two traces from baseline (S1) and monitor (S2) surveys. The time delay is clear between the two traces which can be estimated by solving for m (match filter). The time

delay is a spike, similar to that of a zero phase. Attempting to convert that match filter to minimum phase, time delay estimate will be lost.

SOFTWARE

The platform used to write codes and generate the data is Matlab and many of CREWES toolbox functions are utilized.

ACKNOWLEDGMENTS

The authors would like to thank the sponsors of the Consortium for Research in Elastic Wave Exploration Seismology (CREWES) for their support. Mahdi Almutlaq would like to thank Saudi Aramco for sponsoring his PhD program and their continuous support. He also acknowledges Faranak Mahmoudian for the tips she provided for programming in Matlab.

REFERENCES

Cambois, G., and P. L. Stoff, 1992, Surface-consistent deconvolution in the log/Fourier domain: Geophysics, **57**, 823 – 840.

Cary, P. W., and G. A. Lorentz, 1993, Four-component surface consistent deconvolution: Geophysics, **58**, 383 – 392.

Jack, I., 1998, Time-Lapse seismic in reservoir management: SEG, short course notes.

Levin, S. A., 1989, Surface-consistent deconvolution: Geophysics, **54**, 1123 – 1133.

Morley, L., and Claerbout, J., 1983, Predictive deconvolution in shot-receiver space: Geophysics, **48**, 515 – 531.

Taner, M. T., and Koehler, F., 1981, Surface consistent corrections: Geophysics, **46**, 17 – 22.

Wiggins, R. A., Larner, K. L., and Wisecup, R. D, 1976, Residual static analysis as a general linear inverse problem: Geophysics, **41**, 922 – 938.